Developing Ni_3N/NiO Heterostructure Catalysts to Enhance Hydrogen Evolution Reaction in Alkaline Medium via a Surface-Dependent Mechanism

Fangfang Liu[a], Shan Ji[b*], Yongwei Li[a], Zhihao Fang[a], Vladimir Linkov[d], Yucheng Dong[c*], Hui Wang[c*]

[a] Shandong Engineering Research Center of New Energy Materials and Devices, Weifang University of Science and Technology, 262700, Weifang, China

[b] College of Biological Chemical Science and Engineering, Jiaxing University, 314001, Jiaxing, China

[c] College of Chemical Engineering, Qingdao University of Science and Technology, 266042, Qingdao, China.

[d] South African Institute for Advanced Material Chemistry, University of the Western Cape, Cape Town, 7535, South Africa.

Experimental

1. Materials

Potassium hydroxide (KOH), and hydrochloric acid (HCl) were purchased from China Aladdin Chemical Co., Ltd. All chemicals were of analytical grade and used without further purification. All experimental solutions were prepared using ultrapure water that was produced on a (18.2 MU cm) Milli-Q, Millipore system.

2. Preparation of Ni_3N/NF

The as-prepared $Ni(OH)_2$/NF sample was placed in a porcelain boat and subsequently put into a tube furnace. Initially, the furnace was purged with N_2 for 15 minutes to completely remove residual air. Subsequently, NH_3 was introduced and maintained for 15 minutes with a constant flow rate of 20 mL min^{-1}. The temperature was then raised to 400 ℃ at a heating rate of 10℃ min^{-1} and held at this temperature for 60 mins. The final obtained sample was labeled as Ni_3N/NF.

2. Preparation of NF-N

The pretreated nickel foams were placed in porcelain boat and put inside a tube furnace. First, a purging operation was conducted using N_2 for 15 minutes to thoroughly remove residual air from the tube furnace. Subsequently, ammonia gas was introduced and maintained for 15 minutes, while ensuring a stable flow rate of 20 mL min^{-1}. Then, the temperature was increased at a rate of 10℃ min^{-1} to 400 ℃ and maintained at this temperature for 60 mins. The finally prepared sample was labeled as NF-N.

4. Calculation of TOF

The turnover frequency (TOF) of each active site in the catalyst was calculated according to Equation [2].

$$TOF\left(\frac{H_2}{s}\right) = \frac{\#total\ hydrogen\ turnover\ per\ geometric\ area}{\#actives\ sites\ per\ geometric\ area} \#(1)$$

TOF ($H_2\ s^{-1}$)=Total hydrogen turnover per geometric area/Number of active sites per geometric area.

The total hydrogen turnover is calculated from the current density as follows:

#total hydrogen turnovers

$$= (|j|\ mA\ cm^{-2})(\frac{1\ C\ s^{-1}}{1000\ mA})(\frac{1\ mol\ e^{-1}}{96485\ C})(\frac{1\ mol\ H_2}{2\ mol\ e^{-1}})(\frac{6.02 \times 10^{23}\ H_2\ molecules}{1\ mol\ H_2})$$
$$= |j| \times 3.12 \times 10^{15}\ \mathrm{H_2}\ s^{-1}\ \mathrm{cm}^{-2} \#(2)$$

The number of active sites for the Ni_3N/NF and Ni_3N/NiO/NF catalysts was determined by calculating the atomic amount of Ni_3N loaded on the nickel foam, based on the assumption that one active site corresponds to one metal center.

#active sites

$$\left(\frac{\text{catalyst loading per geometric area } (\text{x g cm}^{-2}) \times \mathrm{Ni_3N\ wt.\%}}{\mathrm{Ni_3N\ Mw\ (g\ mol^{-1})}}\right)(\frac{6.022 \times 10^{23}\ \mathrm{Ni_3N\ atoms}}{1\ \mathrm{mol\ Ni_3N}})$$
$$= (\frac{0.04\ \mathrm{g\ cm^{-2}} \times \mathrm{Ni_3N\ wt.\%}}{190.07\ \mathrm{g\ mol^{-1}}})(\frac{6.022 \times 10^{23}\ atoms}{1\ mol})$$
$$= 1.27 \times 10^{19} \times \mathrm{Ni_3N\ wt.\%\ sites\ per}\ cm^2 \#(3)$$

Substituting Equations (2) and (3) into (1) gets the TOF for the catalyst:

$$TOF = \frac{3.12 \times 10^{15}}{1.27 \times 10^{19} \times \mathrm{Ni_3N\ wt.\%}} \times |j| \#(4)$$

5. Calculation of ECSA

The electric double-layer capacitance of the catalyst was measured at various scan rates using cyclic voltammetry measured in the non-faradaic region:

$$J = v \times C_{dl} \#(5)$$

$$ECSA = \frac{C_{dl}}{C_s} \times S \#(6)$$

Equation (5) describes the determination of the electric double-layer capacitance of the catalyst in the non-faradaic region at various scan rates using cyclic voltammetry. Here, J denotes the double-layer charging current density, v is the scan rate, C_s (μF cm^{-2}) represents the specific capacitance of the electrode surface, and S (cm^2) is the actual surface area of the working electrode.

In Equation (6), the value of C_s in NaOH and KOH solutions typically ranges from 0.022 to 0.130 mF cm^{-2}. A typical value of 0.040 mF cm^{-2} was adopted for calculation in this study.

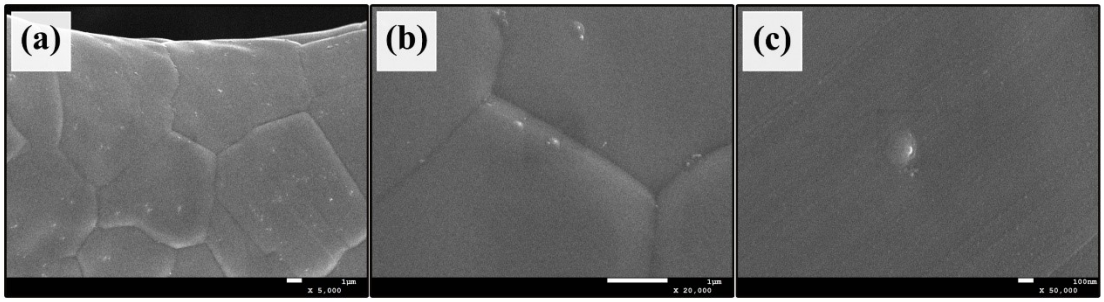

Figure S1. SEM images of NF.

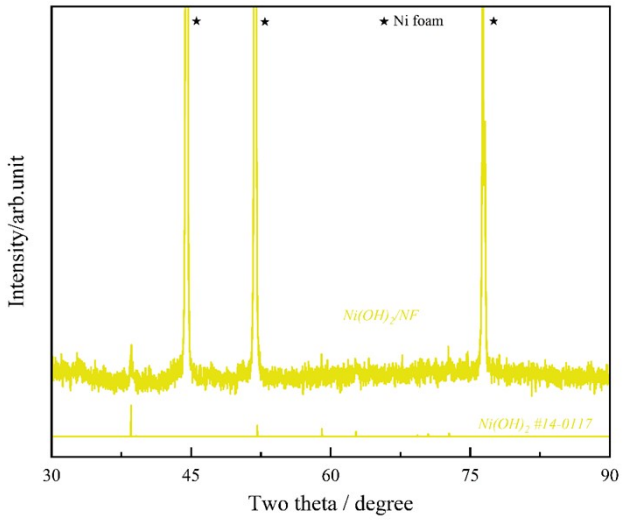

Figure S2. XRD patterns of $Ni(OH)_2$/NF.

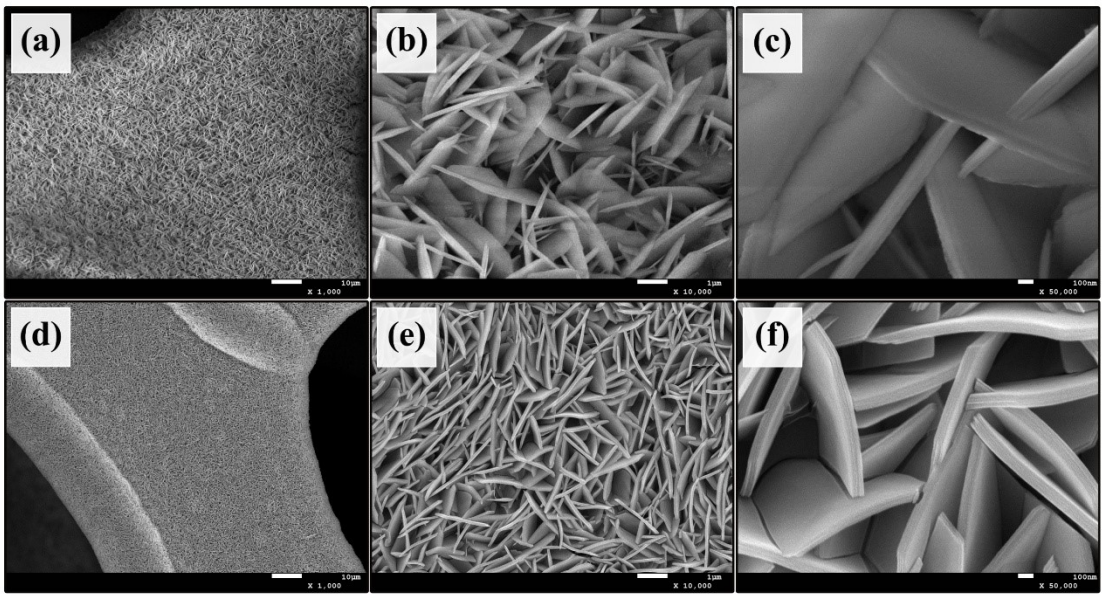

Figure S3. SEM images of (a-c) $Ni(OH)_2$/NF and (d-f) NiO/NF.

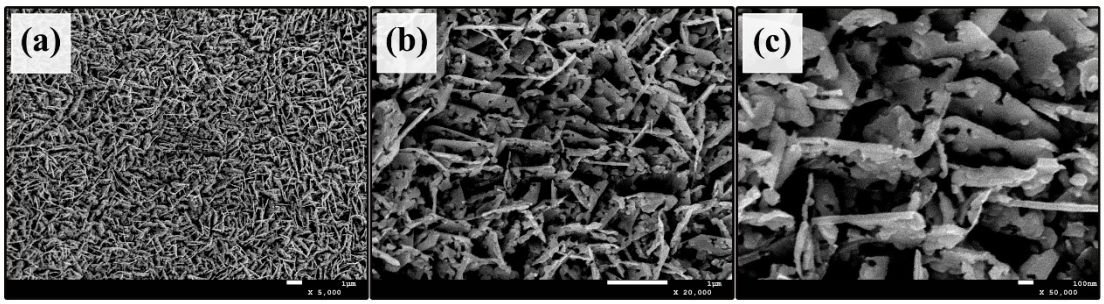

Figure S4. SEM images of Ni_3N/NF.

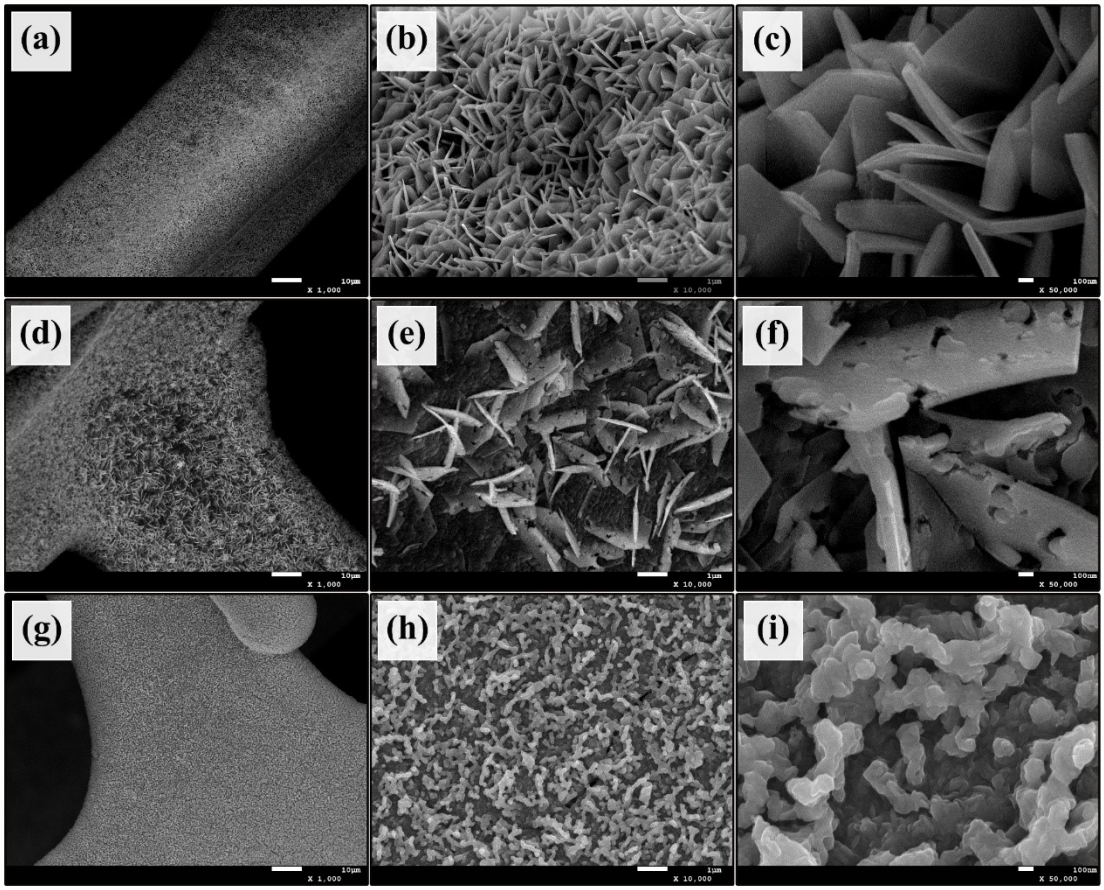

Figure S5. (a-c) SEM images of Ni_3N/NiO/NF-350, (d-f) Ni_3N/NiO/NF-450 and (g-h) Ni_3N/NiO/NF-500.

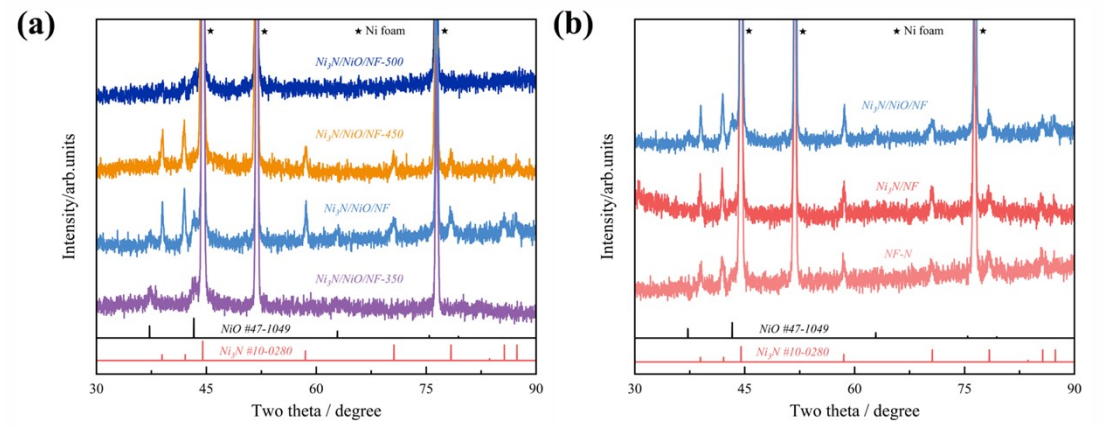

Figure S6. XRD patterns of (a) NF-N, Ni_3N/NF, NiO/NF and Ni_3N/NiO/NF; (b) Ni_3N/NiO/NF-350, Ni_3N/NiO/NF, Ni_3N/NiO/NF-450 and Ni_3N/NiO/NF-500.

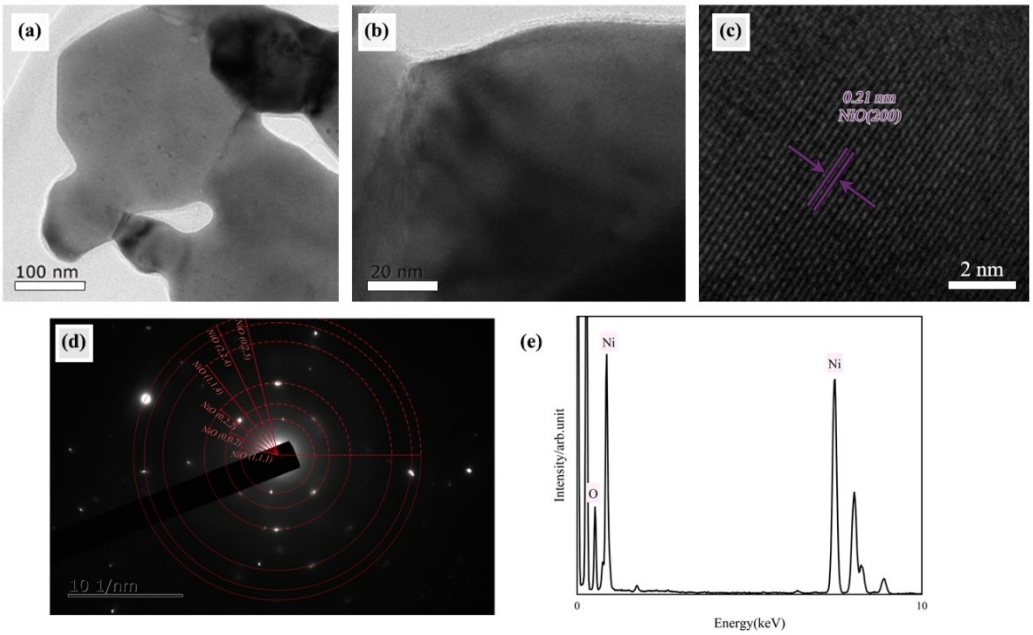

Figure S7. (a) TEM image and (b-c) HR-TEM image; (d) SAED patterns; (e) EDX spectra of NiO/NF.

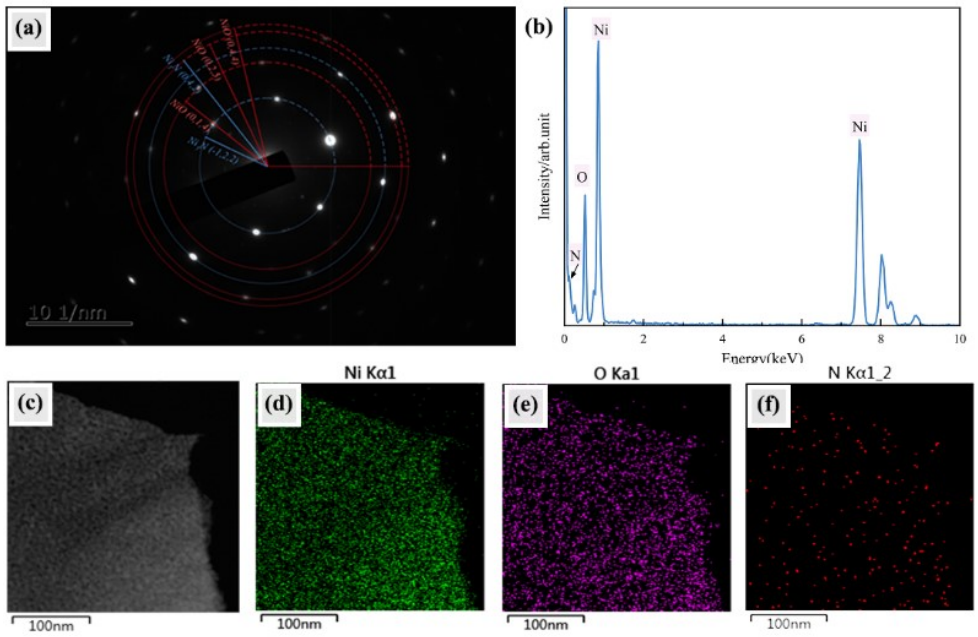

Figure S8. (a) SAED patterns; (b) EDX spectra; (c) STEM and electron energy loss spectroscopy (EELS) elemental mappings of (d) Ni; (e)O; (f) N of Ni_3N/NiO/NF.

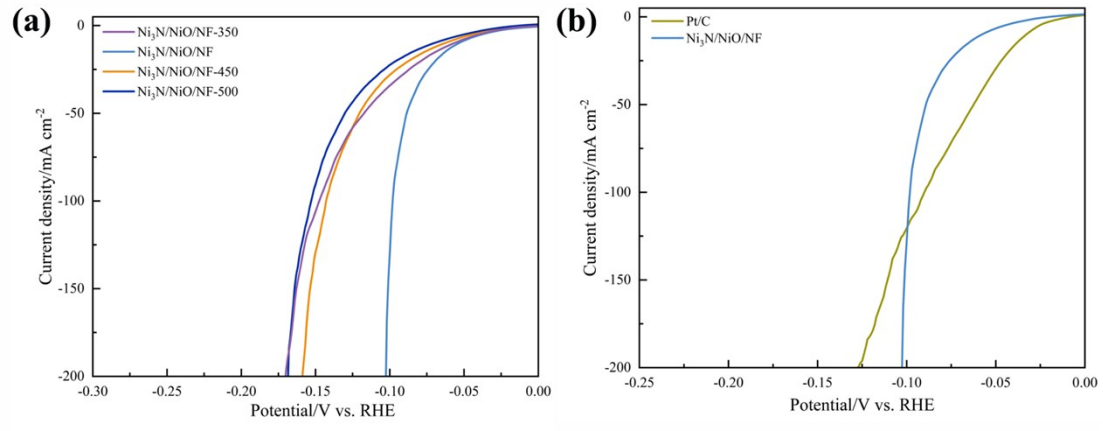

Figure S9. LSV curves of (a) Ni_3N/NiO/NF-350, Ni_3N/NiO/NF, Ni_3N/NiO/NF-450 and Ni_3N/NiO/NF-500; LSV curves of (b) Pt/C and Ni_3N/NiO/NF.

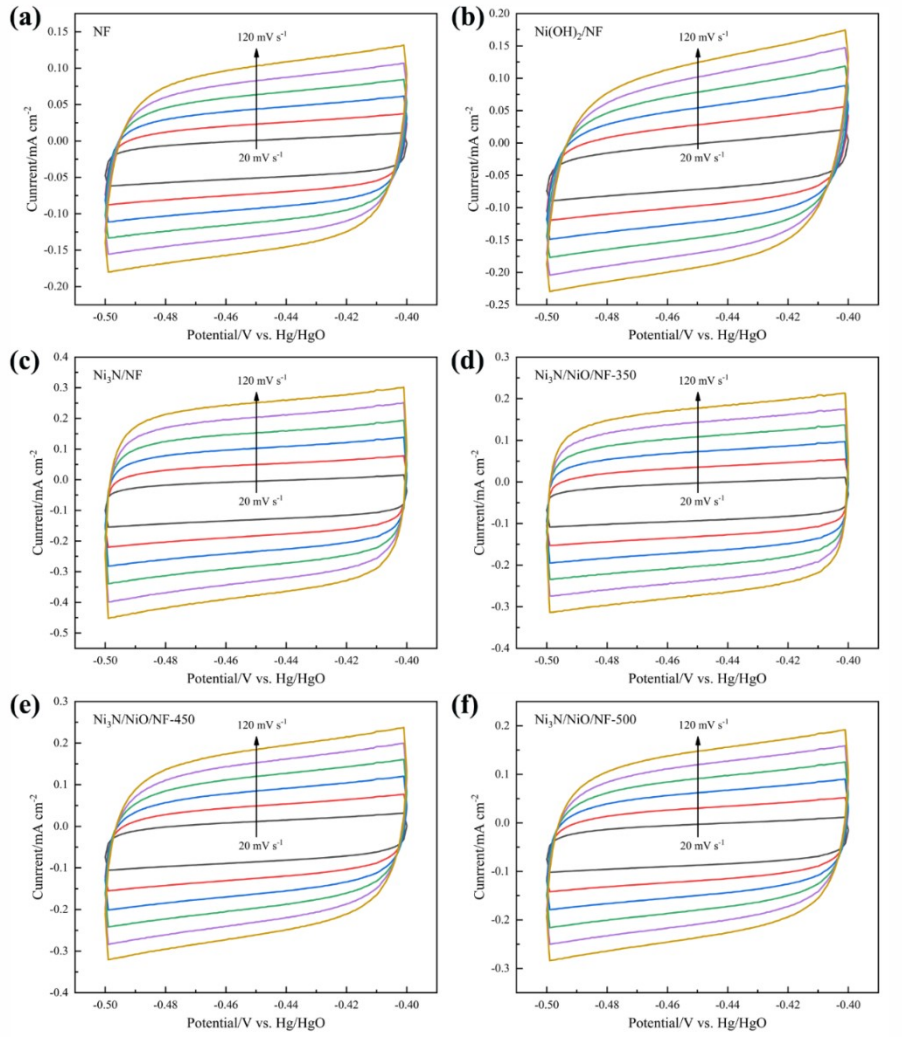

Figure S10. CV curves of (a) NF, (b) $Ni(OH)_2$/NF, (c) Ni_3N/NF, (d) Ni_3N/NiO/NF-350, (e) Ni_3N/NiO/NF-400 and (f) Ni_3N/NiO/NF-500.

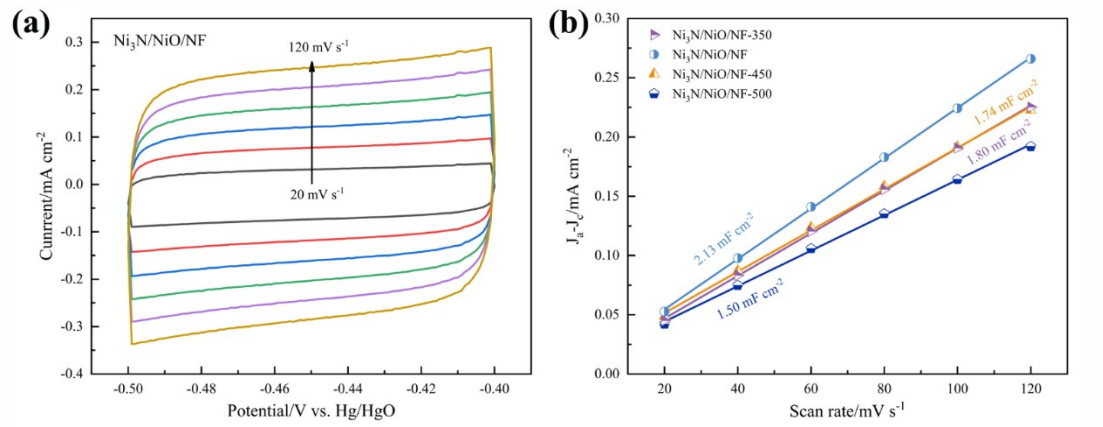

Figure S11. CV curves of (a) Ni_3N/NiO/NF; Linear fitting graph of △j vs. scan rates: (b) Ni_3N/NiO/NF-350, Ni_3N/NiO/NF-450, Ni_3N/NiO/NF-500.

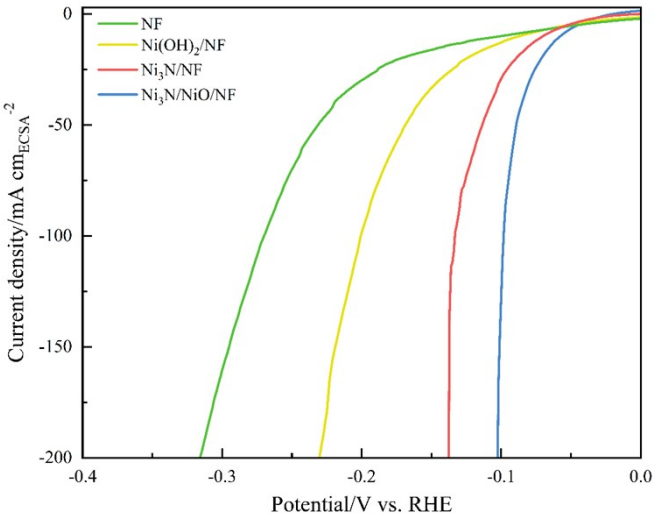

Figure S12. ECSA-normalized LSV curves of NF, $Ni(OH)_2$/NF, Ni_3N/NF and Ni_3N/NiO/NF.

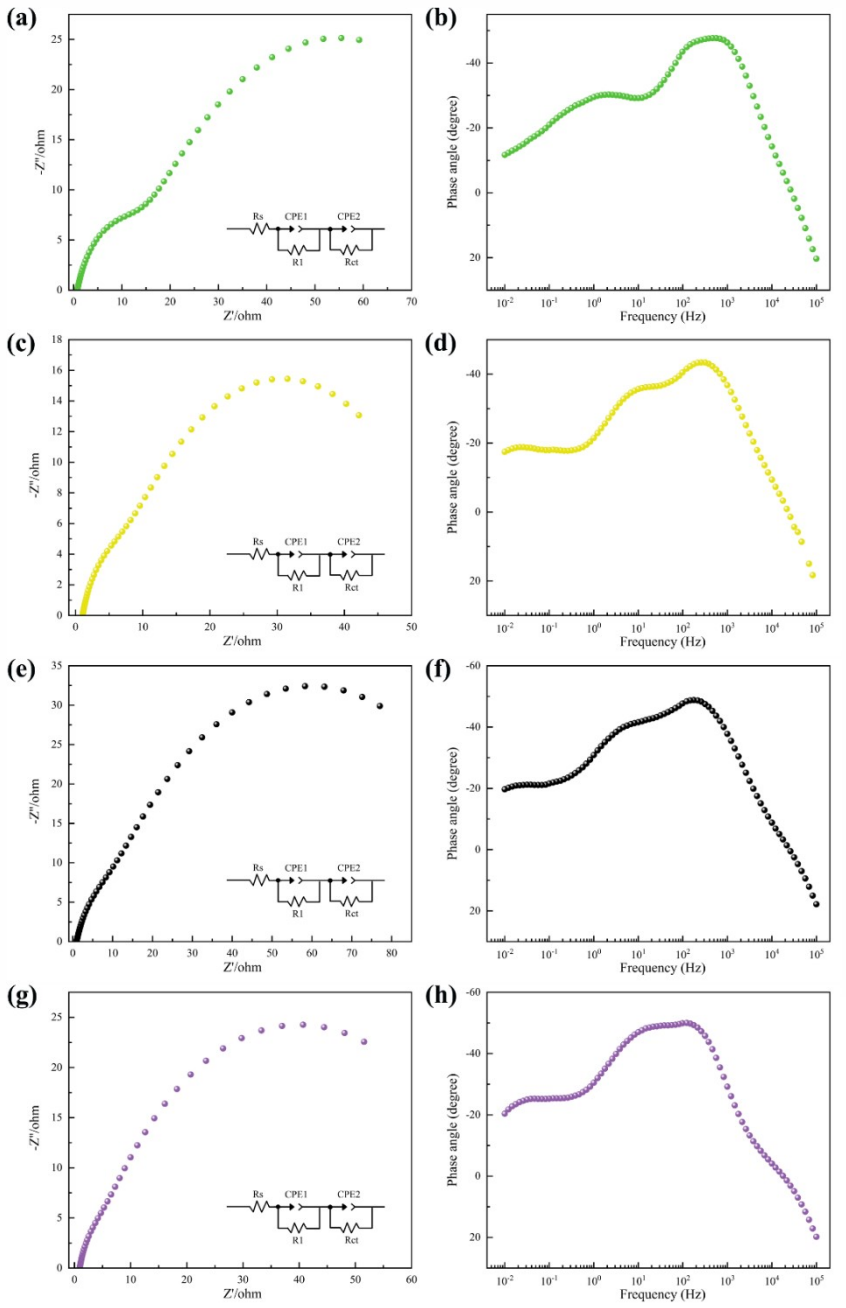

Figure S13. (a) Nyquist plot and (b) Bode plot of NF. (c) Nyquist plot and (d) Bode plot of $Ni(OH)_2$/NF. (e) Nyquist plot and (f) Bode plot of NiO/NF. (g) Nyquist plot and (h) Bode plot of Ni_3N/NiO/NF-350.

Nyquist plot. The inset shows the corresponding equivalent circuit diagram of the two-time-constant serial model, which consists of a series resistance (R_s) and two parallel combinations: resistance R_1 with constant phase element CPE_1, and charge-transfer resistance R_{ct} with constant phase element CPE_2. Here, Rs represents the uncompensated solution resistance; the time constant R_1–CPE_1 is related to the interfacial resistance, while R_{ct}–CPE_2 corresponds to the charge-transfer resistance.[1, 2]

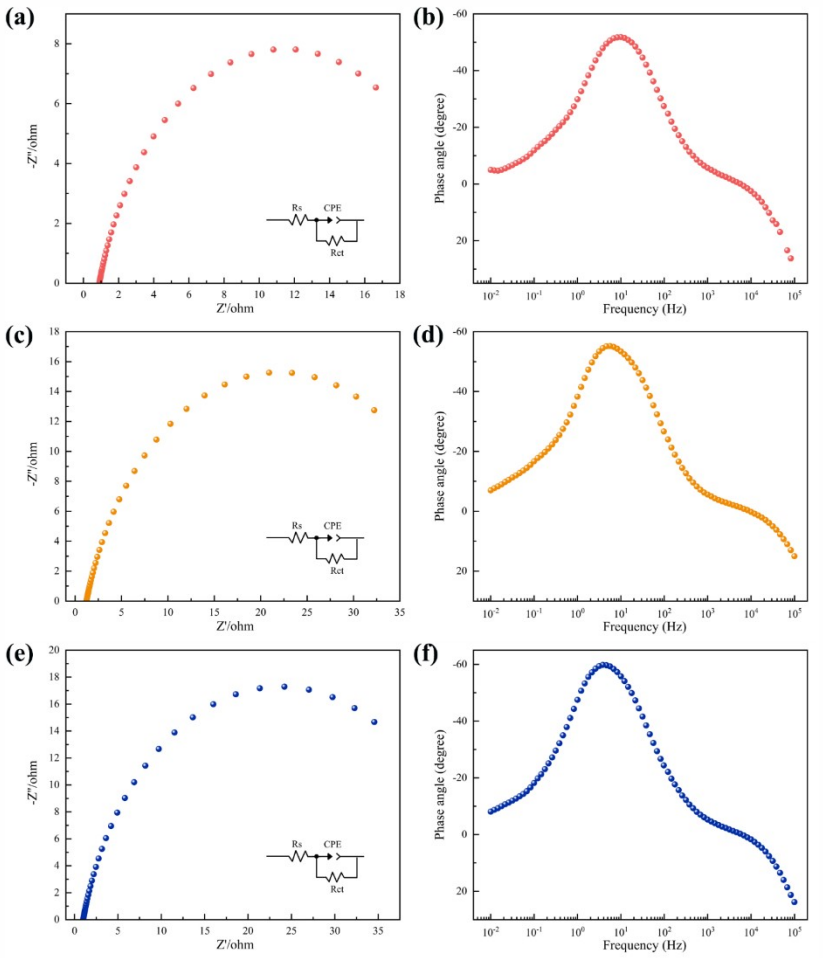

Figure S14. (a) Nyquist plot and (b) Bode plot of Ni_3N/NF. (a) Nyquist plot and (b) Bode plot of Ni_3N/NiO/NF-450. (a) Nyquist plot and (b) Bode plot of Ni_3N/NiO/NF-500.

Nyquist plot. The inset shows the corresponding equivalent circuit diagram of the one-time-constant model, which consists of a series resistance (R_s) and a parallel combination of charge-transfer resistance (R_{ct}) and a constant phase element (CPE). Here, Rs represents the uncompensated solution resistance, while the time constant R_{ct}–CPE is associated with the charge-transfer resistance.

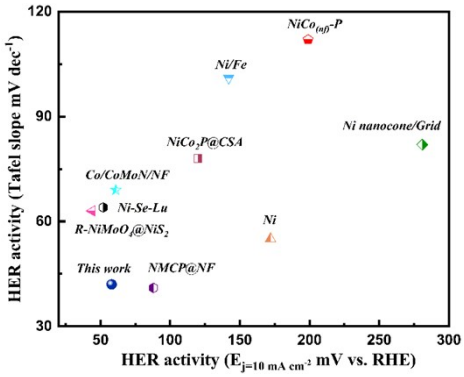

Figure S15. Compare the Tafel slope and the overpotential at 10/100 mA cm^{-2} of the Ni_3N/NiO/NF electrode with those reported for electrocatalysts in the literature.

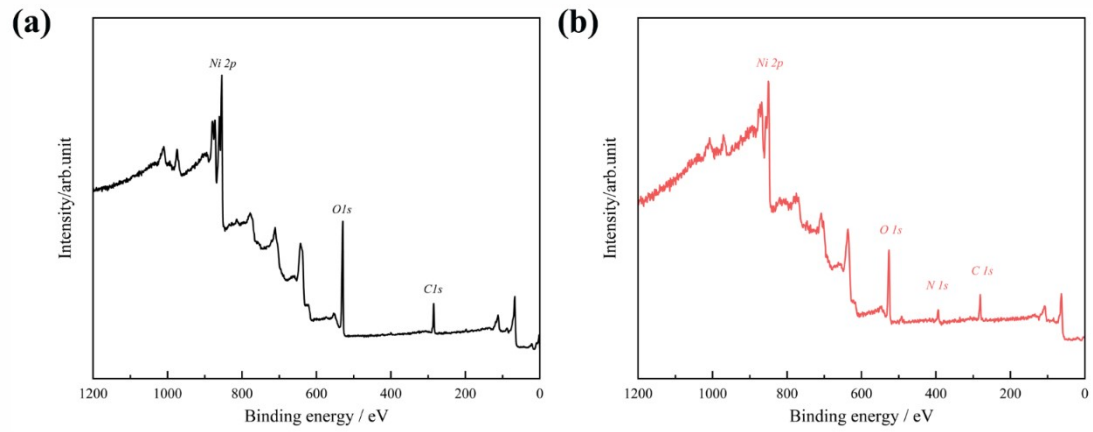

Figure S16. XPS survey spectrum of (a) NiO/NF and (b) Ni_3N/NF.

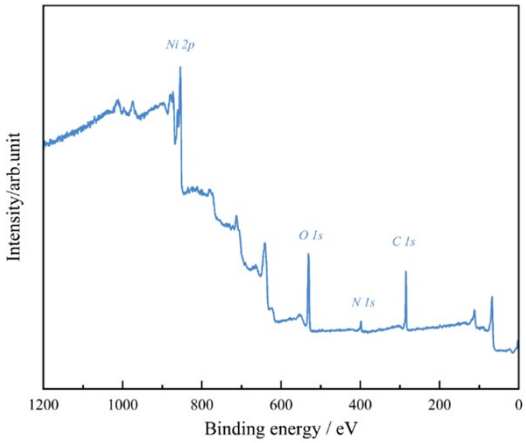

Figure S17. XPS survey spectrum of Ni_3N/NiO/NF.

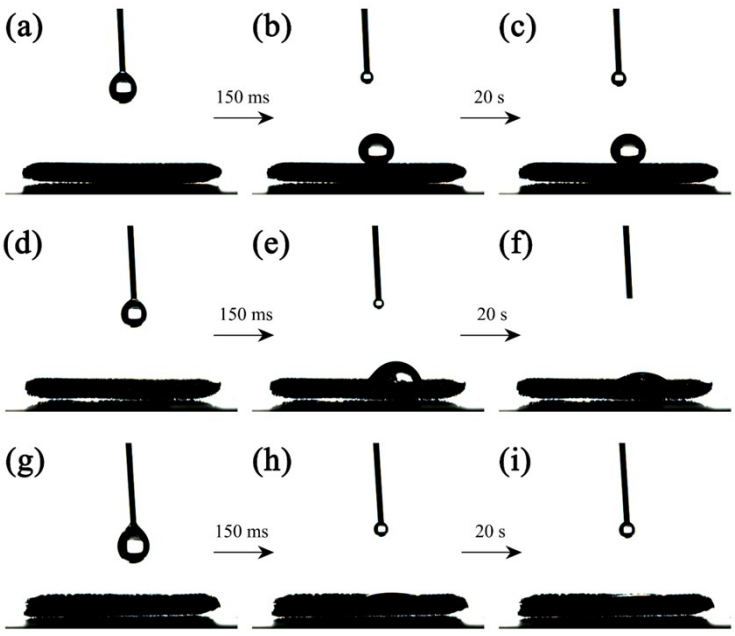

Figure S18. Water wettability tests of (a) NF, (b) $Ni(OH)_2$/NF and (c) NiO/NF.

Figure S19. Digital images of (a) NF, (b) $Ni(OH)_2$/NF and (c) NiO/NF samples during hydrogen evolution at a current density of 50 mA cm^{-2}.

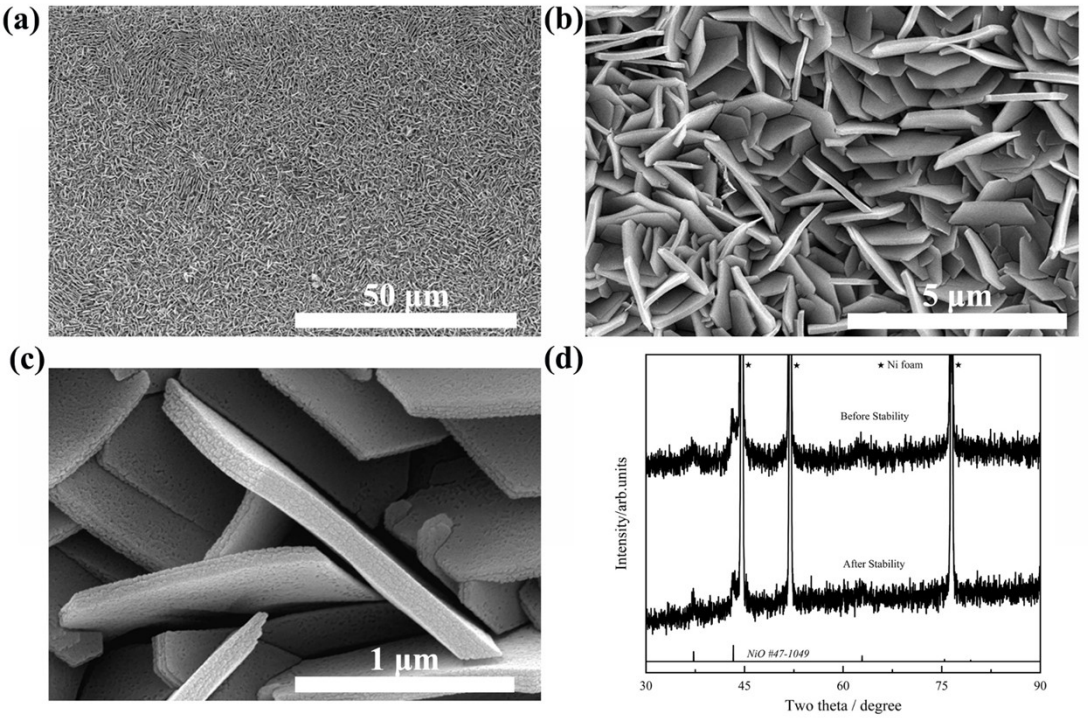

Figure S20. (a-c) SEM and (d) XRD images after CP testing.

Table S1. ECSA of different samples

Sample	ECSA cm^2
NF	25.00
$Ni(OH)_2$/NF	30.50
Ni_3N/NF	62.75
Ni_3N/NiO/NF	53.25
Ni_3N/NiO/NF-350	45.00
Ni_3N/NiO/NF-450	43.50
Ni_3N/NiO/NF-500	37.50

Table S2. Fitting results of the Nyquist plot

Sample	R_s[Ω]	R_1[Ω]	T_1[F s^{n-1}]	n_1	R_{ct}[Ω]	T_2[F s^{n-1}]	n_2
NF	0.8	12.5	0.0007	0.80	83.9	0.0065	0.68
NiO	0.9	6.6	0.0012	0.83	105.3	0.0032	0.70
Ni_3N/NiO/NF-350	0.9	2.7	0.0014	0.94	73.1	0.0029	0.74
$Ni(OH)_2$/NF	1.0	5.2	0.0009	0.83	49.7	0.0036	0.70

Table S3. Fitting results of the Nyquist plot

Sample	Rs[Ω]	Rct[Ω]	T[F s^{n-1}]	n
Ni_3N/NiO/NF-450	1.2	41.6	0.0068	0.81
Ni_3N/NiO/NF-500	1.0	45.5	0.0088	0.83
Ni_3N/NF	0.9	21.1	0.0084	0.81

Table S4. Fitting results of the Nyquist plot

Potential mV	R_s[Ω]	R_{ct}[Ω]	R_2[Ω]	C_ϕ[F]	T[F s^{n-1}]	n
10	0.8	17.4	62.0	0.115	0.0087	0.79
20	0.8	19.0	33.6	0.145	0.0083	0.80
30	0.8	19.4	19.1	0.190	0.0081	0.81
40	0.8	18.7	10.8	0.255	0.0079	0.81

Table S5. ONH analysis of Ni_3N/NF and Ni_3N/NiO/NF

Sample	Nitrogen concentration (%)
Ni_3N/NF	1.33
Ni_3N/NiO/NF	1.04

Table S6. Compare the Tafel slope and the overpotential at 10/100 mA cm^{-2} of the Ni_3N/NiO/NF electrode with those reported for electrocatalysts in the literature.

Electrode	10 mA cm^{-2}	100 mA cm^{-2}	mV dec^{-1}	Ref.
Ni_3N/NiO/NF	58	98	42	This work
W-CoSe300/NF	*	115	53	[3]
$NiCo_2P$@CSA	120	192.4	78	[4]
Ni_3S_2	197	380	159	[5]
Ni	172	*	55	[6]
Ni/NiO	60	181	34	[7]
Ni/Fe	142	239	101	[8]
Ni nanocone/Grid	281	390	82	[9]
GC-CuC	120	*	112	[10]
Ni_3S_2/Ni	236	*	113	[11]
NMCP@NF	88	178	41	[12]
$NiCo_{(nf)}$-P	199	283	112	[13]
Co/CoMoN/NF	61	173	69	[14]
R-$NiMoO_4$@NiS_2	44	146	63	[15]
Ni–Se–Lu	52	*	64	[16]

Mo-NiOH@Fe_3O_4	*	141	107	[17]

1. Z.-Y. Yu, C.-C. Lang, M.-R. Gao, Y. Chen, Q.-Q. Fu, Y. Duan and S.-H. Yu, Energy Environ. Sci., 2018, 11, 1890-1897.

2. H. Jiang, M. Sun, S. Wu, B. Huang, C.-S. Lee and W. Zhang, Advanced Functional Materials, 2021, 31, 2104951.

3. E. Fan, S. Zhou, H. Zhao, J. Ran, Z. Zhang, G. Dong, W. Zhang, Y. Zang, M. Zhao, D.-F. Chai and X. Huang, Dalton Trans., 2024, 53, 10142-10149.

4. F. Wang, M. Xu, J. Ma, Y. Li, J. Zhang, Z. Zhang and S. Min, Dalton Trans., 2025, 54, 12006-12017.

5. G. E. Ayom, M. D. Khan, R. Srivastava, W. Lin, R. K. Gupta and N. Revaprasadu, Dalton Trans., 2025, 54, 14456-14468.

6. L. Jin, Z. Cheng, T. Sun, Z. Gao, L. a. Deng, L. Yang, F. Li, Z. Geng, J. P. Zheng and C. Zhang, J. Power Sources, 2025, 646, 237229.

7. C. Huang, Z. Wang, Z. Yao, Y. Ma, F. Guo and L. Chai, Electrochimica Acta, 2024, 477, 143792.

8. Z. Zhang, Y. Wu and D. Zhang, Int. J. Hydrogen Energy, 2022, 47, 1425-1434.

9. Y. Wen, Z. Zhang, H. Zhu, K. Xu, Y. Zhao, L. Ma and H. Yan, Int. J. Hydrogen Energy, 2024, 89, 518-530.

10. M. M. Ibrahim, G. A. M. Mersal, A. M. Fallatah, K. Althubeiti, H. S. El-Sheshtawy, M. F. Abou Taleb, M. R. Das, R. Boukherroub, M. S. Attia and M. A. Amin, RSC Advances, 2022, 12, 8030-8042.

11. M. Zhu, M. Liu and J. Zhang, RSC Advances, 2024, 14, 29800-29811.

12. M. R. Kandel, U. N. Pan, D. R. Paudel, P. P. Dhakal, N. H. Kim and J. H. Lee, Composites Part B: Engineering, 2022, 239, 109992.

13. Z. Xu, C.-L. Yeh, J.-L. Chen, J. T. Lin, K.-C. Ho and R. Y.-Y. Lin, ACS Sustainable Chemistry & Engineering, 2022, 10, 11577-11586.

14. H. Ma, Z. Chen, Z. Wang, C. V. Singh and Q. Jiang, Adv. Sci., 2022, 9, 2105313.

15. X. Luo, H. Zhao, L. Wang, X. Tan, L. Guo, L. Jiang, M. Wang, Z. Tao and S. Mu, Nano Energy, 2026, 147, 111601.

16. W. Tan, X. Liu, W. Liu, H. He and Y. Yang, Int. J. Hydrogen Energy, 2024, 80, 270-279.

17. B. Li, Z. Cui, Y. Tao, J. Xiong, J. Gao, L. Liu, S. Song and P. Tian, Applied Surface Science, 2026, 720, 165283.